JCAMECH

Vol. 51, No. 2, December 2020, pp 454-463
DOI: 10.22059/jcamech.2020.304872.523

A genetic algorithm-based approach for numerical solution of droplet status after Coulomb fission using the energy conservation method

Mohammad Hamed Hekmat [a,], Morteza Rahmanpour[b], Mahnaz Mahmoudi[b] and Saleh Saharkhiz[a]*

[a] *Department of Mechanical Engineering, Tafresh University, Tafresh 39518-79611, Iran*
[b] *Department of Mechanical Engineering, Azarbaijan Shahid Madani University, Tabriz, Iran*

ARTICLE INFO

Article history:
Received: 21 June 2020
Accepted: 01 September 2020

Keywords:
Genetic algorithm
Droplet
Coulomb fission
Rayleigh limit
Energy conservation method

ABSTRACT

As a droplet moves, due to evaporation at the surface, the droplet size is gradually reduced. Due to decreasing the size of the droplets moving in the spray core, the surface charges become closer and the repulsive force between the charges increases. When the Coulombic force overcomes the surface tension force (Rayleigh instability) the droplet breaks into smaller droplets (Coulomb fission). The present study predicts droplet Coulomb fission and droplets trajectories of steady spray plume in a monodisperse Electrohydrodynamics (EHD) spray within a Lagrangian framework. Droplet fission is simulated based on the principle of minimum free energy using the Genetic Algorithm (GA) and droplet trajectories are predicted using the Lagrangian single-droplet dynamic tracking method. The numerical model is validated by comparing the model predictions with the experimental and previous modeling results. In the current method, an optimization method for minimizing the energy in the minimum energy principle is utilized to avoid any simplifying assumptions, such as number of sibling droplets and charge distribution on their surfaces which may affect the physics of the problem. According to the process of the present solutions and results, it is clearly seen that the developed method has sufficient accuracy and precision.

1. Introduction

In recent years, electrospray is a useful methodology which is used to control the charged droplet generation, and it has a wide range of applications, such as targeted gene delivery, inorganic film formation in solar cells, jet printing, surface coating, and mass spectrometry [1-7]. In the most typical configuration, the liquid is pumped through the capillary at a small flow rate [8]. When an electric potential of the order of kilovolt is applied between the capillary and the ground plate, the droplets are detached from the capillary tip. There are many electrospray modes depending on the nozzle plate configuration, the flow rate, the liquid properties, and the applied voltage [9]. The cone-jet mode is preferred because it stably produces monodisperse droplets. In the cone jet mode, the jet droplets out of the head of the liquid cone meniscus known as the Taylor cone is charged to the droplets. After break-up, the jet leads to particularly electric charged droplets, which passes due to the electrodes through the gaseous phase driven by the electric field and by Coulombic repulsion between the droplets [10].

The first detailed simulation of droplet dynamics in an electrospray was reported by Calvo et al [11]. They solved the equation of motion for each droplet released, which included electric forces from the external field and a Coulombic repulsion and also the drag force due to the friction between the droplets and the gas. The numerical results were compared with the experimental results to show several spatial and statistical properties of the electrosprays. A theoretical model for electrospray droplets transport and evaporation was developed by Wilhelm et al [12]. Also, they examined the effects of evaporation and the presence of a hot impregnated plate on droplet mass and heat transfer. Unlike droplet transport, which is rarely affected by evaporation, droplet size and salt concentration can be affected by evaporation. Oh et al. [13] developed a three-dimensional Lagrangian model to simulate deposition patterns and spray

* Corresponding author. Tel.: +0-863-624-1263; fax: +0-863-624-1264; e-mail: hekmat@tafreshu.ac.ir

evolution. Moreover, they presented the features of two-nozzle electrospray deposition with a capillary–extractor–substrate formation. The results showed that the evolution of the spray was significantly affected by the extraction-substrate voltage but droplet size distribution was not influenced by extraction-bed voltage. Two years later, Jung et al. [14] used this Lagrangian model to predict the deposition patterns which were obtained by transmitting a twin nozzle electro spraying system in parallel with a set plate.

The interaction and overall deposition pattern of multiplexed electrosprays were studied by Yang et al [15]. Space-charge can have a non-negligible effect on some applications with electrospray. They developed a spray profile model to expand a single electrospray source depending on its space-charge field and then generalized to explain the deposition pattern for multiple electrospray sources. The results of numerical simulation and the spray profile model were evaluated with experimental data and good agreement was shown. Jiang et al. [16] presented an improved model due to the effect of charged droplet emitted from the tip of the jet cone on the external electric field. The results showed that by reducing the mean relative error from 12.5% to 4.4%, the accuracy of the improved model could be increased to predict the shape of the jet cone due to the effects of space-charge. Tracing the trajectories of the separated droplets in Lagrangian numerical simulation of the electrosprays requires a large number of calculations. Grifoll et al. [17, 18] proposed an efficient Lagrangian simulation of electrospray droplets dynamics to reduce the CPU time, while preserving accuracy. As the solvent evaporates from the droplets, the charge density on their surfaces becomes higher. Depending on how the charge density is dealt with, the Coulomb force exceeds the surface tension force, and then droplets undergo fission resulting in offspring droplets [19, 20]. Gu et al. [21] modeled Fine Coulomb fission of liquid droplets within the Rayleigh range [22], a limit to the maximum acceptable value on a liquid surface. they combined the theories for the conventional electrostatic spraying and the flow-limited field-injection electrostatic spraying. Further, when Coulomb fission does occur, then mass of the order 1% to 5% is ejected from the parent droplet and the siblings created carrying a charge the order of 15%-20% that of the parent [23-26]. Many authors have examined the dynamics of droplet fission. Roth and Kelly [26] presented a simple model based on mass, charge, and energy conservation between the initial and final states of energy using the following assumptions:

- the starting droplet is at rest;
- the effects of exogenous electric fields are negligible;
- disruption process is isothermal: viscous losses, evaporative cooling, aerodynamic heating;
- wave generation can be neglected;
- evaporation of mass from the parent droplet can be ignored after a disruption occurs;
- the siblings (*n* in number) are all identical;
- siblings were regularly geometrically emitted;

But this model, however, has some limitation as:

- charging and mass loss values were not predicted separately and only their ratio is calculated;
- there is no prediction for the number, size, or charge level of the sibling droplets.

Shrimpton [25] improved the model of Roth and Kelly[26], and presented a better model that had good physical agreement with the nature of droplet fission. They also evaluated the sensitivity of the charge redistribution assumption, and developed an improved model compared with recent empirical evidence. But in this model, assumptions 1, 3, 4, 6, 7 had been retained yet. In particular, the existence of an external electric field, the nature of the liquid dielectric and used photographic evidence as a basis of geometric assumptions had been considered which are physically reasonable. But other hypotheses do not agree with the determinant and repetitive nature of the Coulomb fission process in the Rayleigh limit. Also, the position of the droplets is not calculated after fission, and a simple model is used to estimate the residual and sibling location. Consequently, the present study tries to avoid any simplifications and assumptions using an optimization method for minimizing the energy in the minimum energy principle that may affect the physics of the problem.

2. Analysis

2.1. Droplet transport

The integrated equations of motion of the electrospray droplets into the regular electrode configuration is considered. The motion of the spray droplet *i* is described by the positional vector R_i and the velocity vector V_i, which are functions of time (t), and is obtained by solving its motion equations:

$$\frac{dR_i}{dt} = V_i \tag{1a}$$

$$\frac{dV_i}{dt} = a_i \tag{1b}$$

where a_i is acceleration, that is the sum of forces performing on the droplet *i* and divided by its mass. The motion of the droplets from the electrified nozzle to the counter electrode using the tracing of Lagrangian droplets from the two-phase dilute flow is quantitatively described. The electrospray system is considered to be droplets that do not interfere with each other and only Coulomb force and drag from the surrounding air act on them. Also, air can still be assumed under normal conditions. Thus, a force balance for transport of droplet i is written as [27]:

$$\frac{\pi}{6} d_i^3 \rho_d \frac{d\vec{v_i}}{dt} = C_D \frac{\pi}{8} \rho_g d_i^2 \vec{v_i}^2 \vec{e_i} + q_i \vec{E}_{ext} + \frac{1}{4\pi\varepsilon_0} \sum_{ij,i\neq j}^{N} \frac{q_i q_j}{R_{ij}^3} \vec{R}_{ij} \tag{2}$$

where d_i is the droplet diameter (m), ρ_d is the liquid density (kg/m^3), ρ_g is the air density (kg/m^3), C_D is the drag coefficient, q_i is the electrical charge carried by i^{th} droplet (C), $\vec{E}_{ext}$ is the external electrical field vector that created by the potential difference between the capillary tube and the plate (V/m), $\vec{R}_{ij} = \vec{R}_i - \vec{R}_j$ is displacement between the position vectors of droplets j ($\vec{R}j = (r_j, z_j)$) and i (m), ε_0 is the air permittivity (taken as 8.854×10^{-12} A.s/V.m), and N is the total number of droplets. The right-hand side terms of Eq. (1) account for the drag force by the surrounding gas, the force on the droplets by the external electric field $\vec{E}_{ext}$ between the nozzle and the grounded plate, and the mutual electric forces between the charged droplets respectively. The C_D drag coefficient is written as follows [27]:

$$C_D = \frac{24}{Re}(1 + 0.15\, Re^{0.678}) \qquad Re < 800 \tag{3}$$

In this work, the droplets are assumed to move in still air as considered in the study of Calvo et al.[11].

2.2. Primary break-up model

The initial condition for the integration of Eq. (1) is taken as the velocity of the jet before the primary break-up. The jet velocity is estimated from the flow rate of the liquid to be sprayed and the jet diameter. This jet diameter is obtained from the numerical modeling of Taylor cone jet formation in Electrospray [28]. The jet becomes unstable due to disturbances, and its wavelengths (λ_{opt}) are [29]:

$$\lambda_{opt} = \sqrt{2}\pi d_0 \left(1 + \frac{3\mu_d}{\sqrt{\rho_d \sigma d_0}}\right)^{0.5} \quad (4)$$

where μ_d and σ are dynamic viscosity of droplet and surface tension of the liquid droplet, respectively and d_0 is the jet diameter of liquid. In this work, according to [11], the droplet emission point is considered to be separate from the end of the capillary tube by a height of the Taylor cone plus three wavelengths.

Very little empirical data on droplet size in electrostatic atomization are available in the published literature. Mori et al. [30] proposed the following correlation for the mean droplet size SMD generated in the electrostatic atomization:

$$SMD = 5.39 d_0 \bar{E}^{-0.255} \bar{V}^{0.277} Re^{-0.124} \quad (5)$$

with $\bar{E} = \epsilon E^2 d_0/\sigma$, $\bar{V} = \rho_d \dot{V_d}^2/(\sigma {d_0}^3)$ and $Re = \rho_d \dot{V}_d/(\mu_d d_0)$ where ϵ is the dielectric constant. Clearly, the mean droplet size decreases with increasing electric field intensity, dielectric constant, and liquid surface tension, but increases with increasing liquid flow rate, liquid density, liquid viscosity, and liquid supply tube diameter. The effects of fluid surface tension and fluid supply tube diameter are less pronounced on electrostatic atomization [31].

In many atomization processes of normal liquids and liquid atomization processes, the droplet size distribution in the primary breakup process is relatively consistent with the lognormal distribution. The values of both of these parameters can be easily determined from the experimental data plot (cumulative weight percent versus droplet size) on a log-probability graph paper. In this study, the mean droplet size found from Eq. (5) and used 4% for standard deviation according to experimental results.

2.3. Droplet evaporation

The problem of evaporation of a single liquid droplet in a stationary environment is just Stephen's problem [32] for the symmetric spherical coordinate system. The droplets expose to evaporation on their trajectory from the nozzle to the counter plate and their size decreases during transportation. The droplet radius history is obtained by writing the mass balance, which states that the rate of droplet mass decreases by the amount of liquid evaporation:

$$\frac{dm_d}{dt} = -\dot{m} \quad (6)$$

where the droplet mass, m_d, is given by:

$$m_d = \rho_d \pi {d_d}^3/6 \quad (7)$$

and d_d is the droplet diameter. According to the Stefan problem for single droplet evaporation, the evaporation rate is expressed as [30]:

$$\dot{m} = 4\pi r \rho D_{AB} ln(1 + Y_B) \quad (8)$$

where Y_B and D_{AB} are the dimensionless transfer number and diffusion coefficient, respectively. By substituting Eq. (7) and (8) to Eq. (6), and performing the differentiation yields the evaporation rate as follows:

$$\frac{dd_d}{dt} = -4\frac{\rho_a}{\rho_d}\frac{D_{AB}}{d_d} ln(1 + Y_B) \quad (9)$$

All properties of the air-solvent gas mixture in the film boundary layer around the droplet can be assumed constant if they are all calculated at reference temperature and composition. These values are estimated by Rule 1/3 [30].

2.4. Electric field equations

The study of the effect of electric field on dielectric media requires knowledge in the field of electric field distribution as well as electric potential. In principle, the distribution of electric potential in a system under applied electric fields may be determined using the Poisson equation, provided that the dielectric constant is kept constant [28-33]:

$$\nabla^2 \phi = -\frac{q_s}{\varepsilon} \quad (10)$$

where ϕ, q_s, ε, respectively, indicate the electric potential, the space charge density, and the electrical permittivity. In the case of dielectric fields, there is no bulk charge density unless a specific element of the dielectric medium is traced to a charge source through its streamline. If so, the Poisson equation is reduced to the Laplace equation:

$$\nabla^2 \phi = 0 \quad (11)$$

The quasi electrostatic case is considered where the magnetic flux $\vec{B}$ does not change over time.

Due to Faraday's law of induction, the curl of electric field disappears:

$$curl\ \vec{E} = \nabla \times \vec{E} = 0 \quad (12)$$

According to Eq. (12), the non-rotational nature of the electric field intensity indicates that there is a scalar function (electric potential) related to the electric field intensity:

$$\vec{E} = -\nabla \phi \quad (13)$$

In this study, Eq. (11) is solved for the nozzle geometry and the plate with a distance of *H* between them. Moreover, a high potential ϕ_0 is applied between the nozzle and the extractor and the electric field intensity is calculated with Eq. (13).

3. Coulomb fission break-up model and governing equations

3.1. Energy balance

The charges in the droplets are distributed on their surfaces over equal spacing to minimize potential energy [34]. Two forces are acting in opposite directions in the charged droplets. One is the surface tension of the charged droplets, which tries to maintain the spherical shape of the droplet, and another force is the Coulomb force of repulsion between similar charges on the surfaces, which tries to break down a spherical charged droplet [35, 36]. Solvent evaporation occurs when droplets pass through the space between the capillary and the spray nozzle. As a result, the size of the droplets decreases until they reach the Rayleigh limit. Where surface traction can no longer maintain the repulsive force of the Coulomb force, and at this point "Coulomb explosion" or "Coulomb fission" occurs; that is, the parent droplet breaks up into much smaller offspring droplets[37]. The schematic diagram of the droplets and Coulomb fission is shown in Fig 1. Rayleigh limit is first defined by Lord Rayleigh as follows [22]:

$$q_i \geq 8\pi\sqrt{\varepsilon_0 \gamma R_i^3} \quad (14)$$

where γ is the surface tension. Also, it is assumed that volume changes in parent droplet and offspring's droplets due to evaporation are negligible, which is instantaneous. In the other hand, the fission process assumed to occur suddenly. Considering that each primary droplet *i* is broken into *n* secondary droplets, the total volume ($\forall_i$) and the total electric charge (q_i) will be constant according to the mass and charge continuity:

$$\forall_i = \frac{4}{3}\pi \sum_{k=1}^{n} R_k^3 \quad (15)$$

$$q_i = \sum_{k=1}^{n} q_k \quad (16)$$

where k represents each of the secondary droplets. The most probable number of offspring's droplets and their size is determined by the principle of minimum free energy. The total energy of an offspring's droplets system is determined by calculating energy for the following reasons:

- mutual interactions between the offspring droplets (W_{ci})
- external electric field effects (W_{ei})
- surface energy of the droplets (W_{si})

The energy due to the mutual interactions between the offspring droplets produced from i^{th} droplet (i^{th} parent droplet) is given by [24]:

$$W_{ci} = \frac{1}{4\pi\varepsilon_0} \sum_{k=1}^{n} \sum_{t=k+1}^{n} \frac{q_k q_t}{|\vec{r}_k - \vec{r}_t|} \quad (17)$$

and external electric field energy is:

$$W_{ei} = -\sum_{k=1}^{n} q_k \left(\vec{E}_{ext} . \vec{r}_k\right) \quad (18)$$

The surface energy of each of the offspring droplets is a function of its surface area:

$$W_{s-i} = \sum_{k=1}^{n} \gamma_k S_k \quad (19)$$

where γ_k is the specific surface energy and S_k is the surface area of offspring droplet. So, the total free energy of a system of the offspring charged droplets is

$$W_i = W_{ci} + W_{ei} + W_{si} \quad (20)$$

The droplet fission occurs in such a way that the sum of the total free energy of an offspring droplets' system is minimal, which is the principle of energy-minimization and actually, derives from the second law of thermodynamics. A computational code has been created in FORTRAN that can solve the dynamic equations of motion of the droplets (Eq. (2)) and Eq. (15) to (19) to find the number, position and size of the droplets before and after the droplet fission process. To minimize Eq. (20), a genetic algorithm constrained optimization method is used. Therefore, for the Genetic Algorithm code, the cost function is defined as:

$$Cost\ Function = \frac{1}{4\pi\varepsilon_0} \sum_{k=1}^{n} \sum_{t=k+1}^{n} \frac{q_k q_t}{|\vec{r}_k - \vec{r}_t|} - \sum_{k=1}^{n} q_k \left(\vec{E}_{ext} . \vec{r}_k\right) + \sum_{k=1}^{n} \gamma_k \pi {d_k}^2 \quad (21)$$

However, the used genetic algorithm should be constrained and the following conditions must be satisfied:

$$Subjects: \begin{cases} \forall_i = \frac{1}{6}\pi \sum_{k=1}^{n} d_k^3 \\ q_i = \sum_{k=1}^{n} q_k \end{cases} \quad (22)$$

The design variables include n (number of secondary droplets), q_k , d_k and $\vec{r}_k$ which generated randomly in the first generation and considered the conditions (22). Their range of variations are as follows:

$$2 \le n \le 100 \quad (23a)$$

$$0 \le q_k \le q_i \quad (23b)$$

$$0 \le d_k \le d_0 \quad (23c)$$

$$0 \le r_k \le 2 \times d_i \quad (23d)$$

where d_i is the breakup radius that obtained from the drop separation distance defined in the below equation [26]:

$$d_i = a\cosh(x_1/a)[\cosh(x_1/a) - 1] + x_1 + a\sinh(x_2/a)[\cosh(x_2/a) - 1] + x_2 \quad (24)$$

where

$$x_k = a\cosh^{-1}\left[\frac{1+(1+4r_k/a)^{\frac{1}{2}}}{2}\right], \qquad k = 1, 2 \quad (25)$$

In this equation, it was assumed that each secondary droplet is joined to the parent droplet by a catenary surface of a cross-sectional form a cosh(x/a). This is the minimum connection surface, stating that the available energy of the electrostatic potential is transferred to the kinetic energy, not the surface energy, preferentially. The catenary parameter is selected to maximize the d_i when the surface reaches zero thickness at its minimum. This distance is used as the best estimation in the first generation in the genetic algorithm (GA).

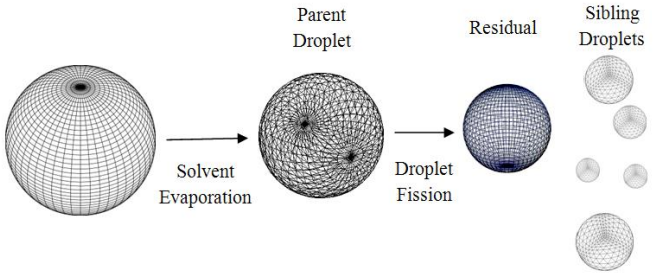

Figure 1. Schematic diagram of the droplet dynamics and fission.

In GA, first several answers are randomly generated for the problem by considering the conditions (22). This set of answers is called the initial population. Each response is called a chromosome. Then, using GA operators, after selecting the best chromosomes (elitism) (the scaling method is used in this work), the chromosomes can be combined and mutated. Finally, the current population is combined with the new population that results from the combination and mutation in the chromosomes. Because GA is based on population production and testing, the possible answer to this problem is inconspicuous, and it is not clear which of the generated solutions are the optimal solution to define the termination condition for finding the best generation. For this reason, we usually keep one of the following termination conditions:

- when there has been no improvement in the population for iterations.
- when we get to the exact number of generations.
- when the value of the objective function has reached a certain predefined value.

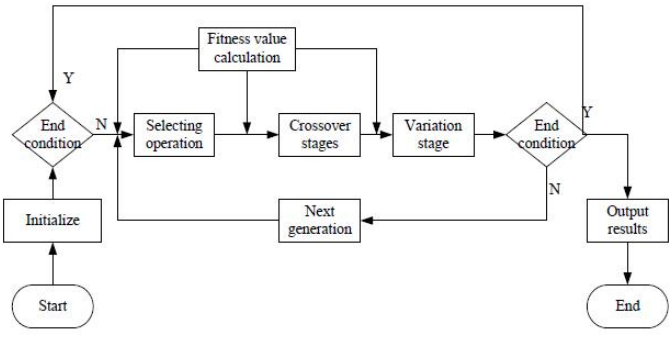

Figure 2. The flowchart of genetic algorithm [38].

Like other GA parameters, the termination condition is a very specific problem, and the GA designer should try different options in order to see what is the best solution for this particular problem. In this work, the second condition is found as the best. Further, for

the velocity of the droplets, it is assumed that to be equal to the initial droplet velocity, but the direction is in line with the remaining droplets and the droplet of the child. Also due to the presence of mutual gravity and repulsion of the charged droplets, possible responses regarding the placement of child droplets in the upstream of fission point are neglected, and only positions for splitting droplets in the direction of spraying are accepted (Figure 1). The GA flowchart is shown in Figure 2. For more details, refer to [38].

4. Results and discussions

At first, for validation, a single droplet of pure Diethyl phthalate (DEP) and pure Dimethyl phthalate (DMP) was simulated numerically with the newly developed model for droplet fission at Rayleigh limit. Some physical properties of DEP and DMP are listed in Table 1. In order to verify the accuracy of the numerical results obtained from the FORTRAN code, the results of the present study are compared with the experimental results of the Millikan Oil Testing Machine which was done by Hunter [39].

Table 1. DEP and DMP specification at 20℃ [39]

Compound	DEP	DMP
Dielectric constant (ε_r)	7.86	8.66
Density (ρ)	1118 kg/m^3	1175 kg/m^3
Viscosity	0.0105 $kg/m.s$	0.0144 $kg/m.s$
Surface tension (γ)	36.1×10^{-3} N/m	40.5×10^{-3} N/m
Electric conductivity (K)	48.6 $\mu S/m$	47 $\mu S/m$
Initial droplet diameter range in Coulomb fission in the relevant Rayleigh Limit	$1.6 - 26$ μm	$21.6 - 38.5$ μm

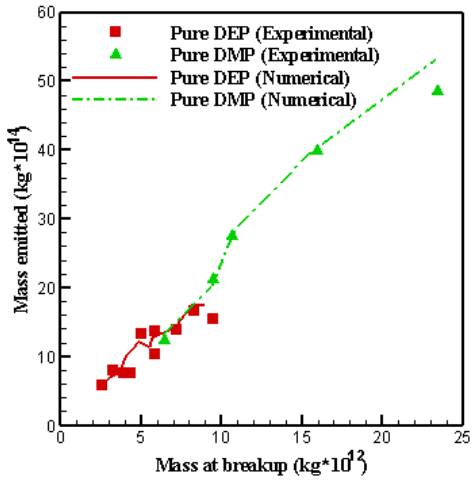

Figure 3. Comparison of the amount of mass emitted for DEP and DMP in the Coulomb fission in the relevant Rayleigh Limit. (Experimental results from Ref. [39])

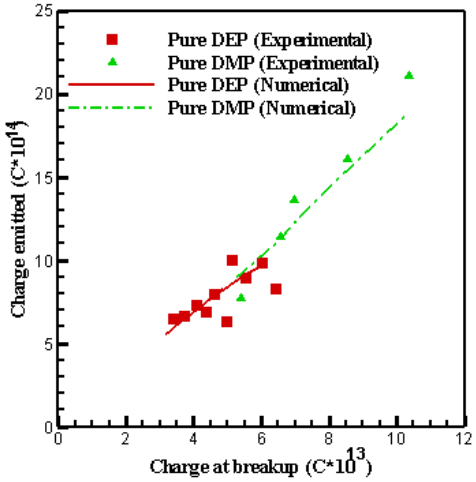

Figure 4. Comparison of the amount of electric charge emitted for DEP and DMP in the Coulomb fission in the relevant Rayleigh Limit. (Experimental results from Ref. [39])

Figure 3 compares the amount of mass emitted at the moment after the Coulomb fission of the droplets with different masses when broken up for both materials. As can be seen, the numerical results are in good agreement with the results of Hunter. It can be seen that in small droplets the difference between numerical and experimental results is negligible and is less than 1.5%. In larger droplets, the difference is slightly larger, reaching a maximum of 5%, which provides a more accurate forecast than the results of other researchers. For the same two materials, Figure 4 also indicates the amount of electric charge emitted in the fission process. But in the emitted charge there is a little more difference and in larger droplets it reaches 20%. It is clear that the agreement of the results is good. But the numerical model for DMP in higher electric charges always overestimates the amount of emitted charge, which is mostly due to the Hall Effect, or the discharge of the electric charge to the plate electrode, which has also been observed by Hunter.

In Figure 5, the amount of mass and electric charge percentage that emitted in the fission process is shown. According to the results, for both materials, the mass emission rate is about 2 to 5% and is about 20% for the charge. It seems that the difference may be due to the purity of the material, the accuracy of the measurement equipment of laboratory and changes in the properties of the material during the fission process, which is also mentioned by the reference. However, the accuracy of the results for engineering predictions is reasonable. The amount of mass and charge emitted is not affected by the initial charge and the primary mass and material properties seem to play an important role. Different materials result in different amounts of mass and charge emitted, while the same material emits almost the same mass and charge under different conditions.

Meanwhile, one of the methods used to test the accuracy of the present numerical method is to compare the amount of mass and electric charge emitted by the Millikan oil droplet-test apparatus, which has been done by various previous researchers. A comparison of the results shows a very good accuracy of the mass

and charge emitted in Coulomb fission in the corresponding Rayleigh Limit. In this numerical study, due to the lack of experimental data about during the process of Coulomb fission in a spray, the developed numerical code was implemented for a single-droplet of water.

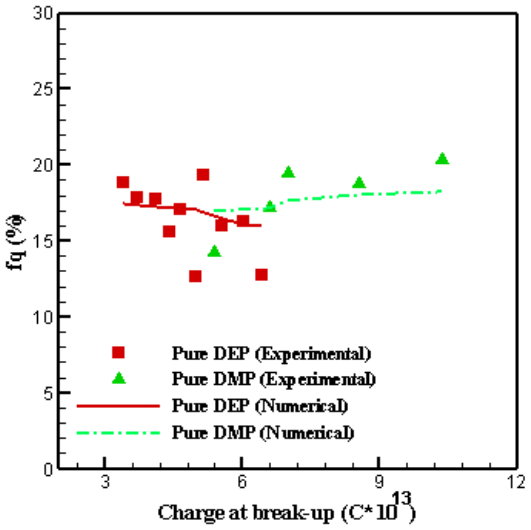

(a)

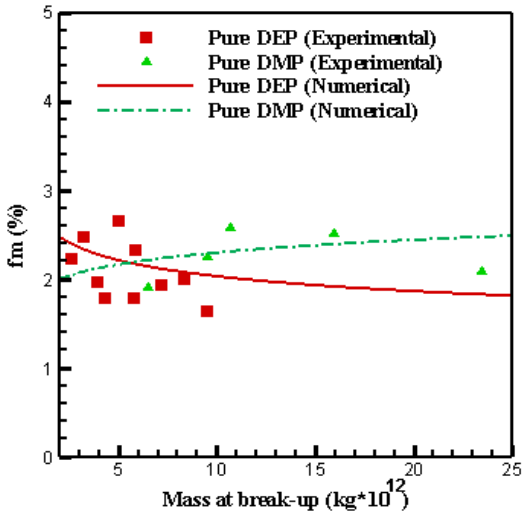

(b)

Figure 5. Comparison of the amount of (a) charge and (b) mass percentage emitted in the Coulomb fission in the relevant Rayleigh Limit. (Experimental results from Ref. [39])

Approximate results for this case are available from reference [40], which is depicted in Figure 6(a). In this experiment, the size of the droplet radius is about 0.9 Rayleigh limit, and the parent droplet radius is assumed to be 0.7 Rayleigh limit just after the Coulomb fission. For this purpose, three stages of evaporation are considered, and the number of droplets of the child due to the Coulomb fission is assumed to be 5, and their sizes are considered the same. After using the code for single droplet simulation with the same reference conditions [40], the following results are obtained and the pattern is shown in Figure 6(b). In the current method, no simplification or default is used. As can be seen, the amount of mass and charge emitted is consistent with experimental results. According to a satisfactory result, this method could be extended for simulating the Coulomb fission process at the Rayleigh limit for droplets in the spray.

Figure 7(a) also displays a comparison of droplet size distribution at $z^* = 1$ for both states without and including Coulomb fission. As can be seen with the Coulomb fission, the number of smaller droplets, which are about 1-3% of the parent droplets, has greatly increased. Therefore, it can be concluded that the spray is almost integrated and the size distribution of smaller droplets is more than the larger droplets. In Figure 7(b), to illustrate the better distribution of droplets, the size of the droplets is zoomed in at 0-0.8μm range, so the range of droplet accumulation is completely clear in this range. Moreover, the Lognormal distribution of droplets can be seen in this diagram which is qualitatively consistent with the experimental results. Also, it could be concluded that considering Coulomb fission is very important in determining the final diameter of droplets in electro-hydrodynamic sprays and can have a great impact on the results.

To better understand the Coulomb fission process and to illustrate the events that occurred in this break-up, methanol electrospray is modeled with the specifications listed in Table 2. In this case, the discharge flow is Q = 4.8 μl /min and the applied voltage is 3 kV. After the cone jet and the connecting jet are formed, the primary break-up modeling is performed, which results in the production of a droplet with an initial diameter of 3.8 μm and an electric charge has been traced from the initial 43,560 times to reach the ground (bottom plate). During the droplet movement, the droplet is affected by the electric field, drag force, and evaporation.

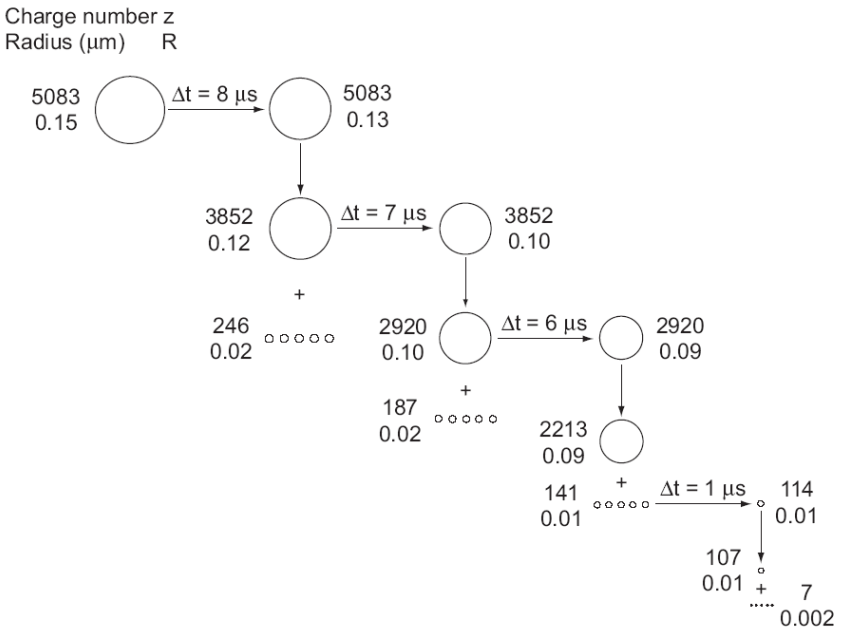

(a)

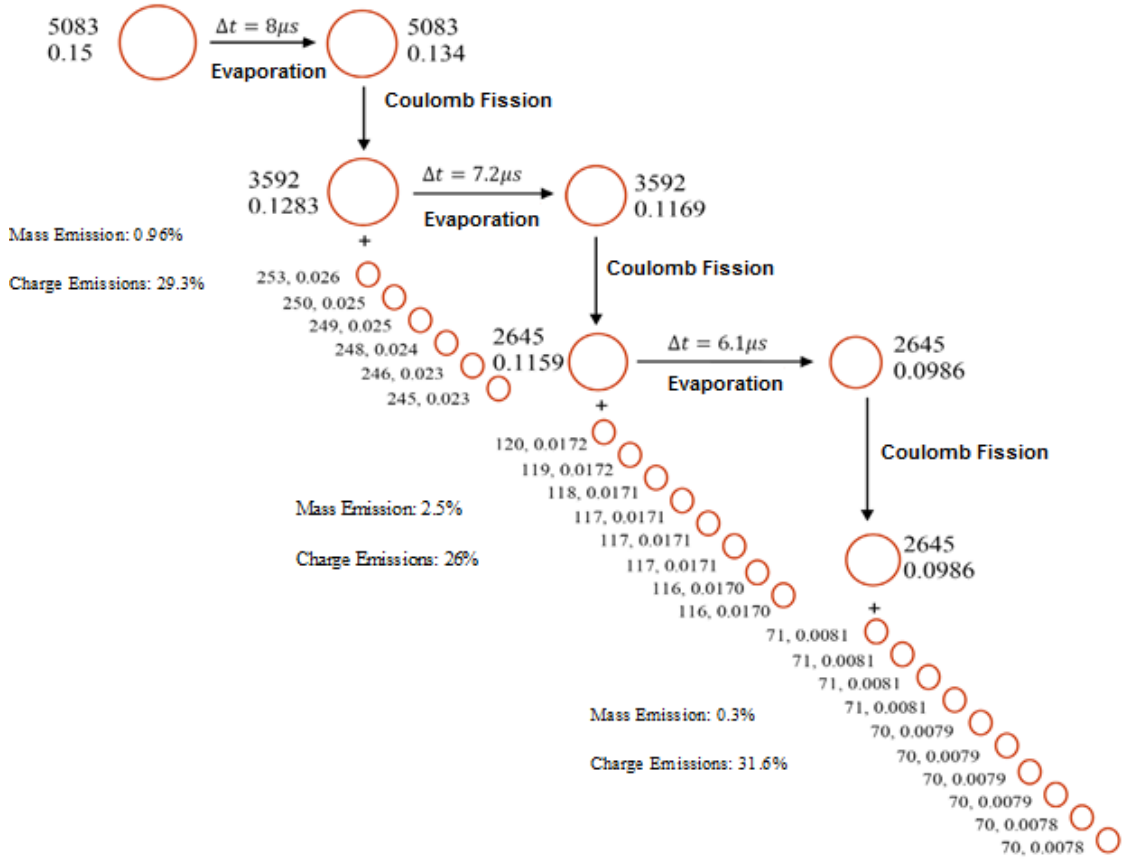

(b)

Figure 6. History of evaporation and Coulomb fission of charged water droplets produced by the nano spray process (a) presented by Kebarle et al. [40] and (b) modeled by the present genetic algorithm and principle of minimum energy.

Due to the evaporation of the droplets, the surface-to-volume ratio has increased. As a result, the rate of evaporation increases and the droplet rate decreases faster.

Table 2. Methanol specification at 20℃

Dielectric constant (ε_r)	32.66
Density (ρ)	791.80 kg/m^3
Dynamic viscosity (μ)	0.593 MPa
Surface tension (γ)	22.5 dyn/cm
Electric conductivity (K)	7.0 $\mu S/m$

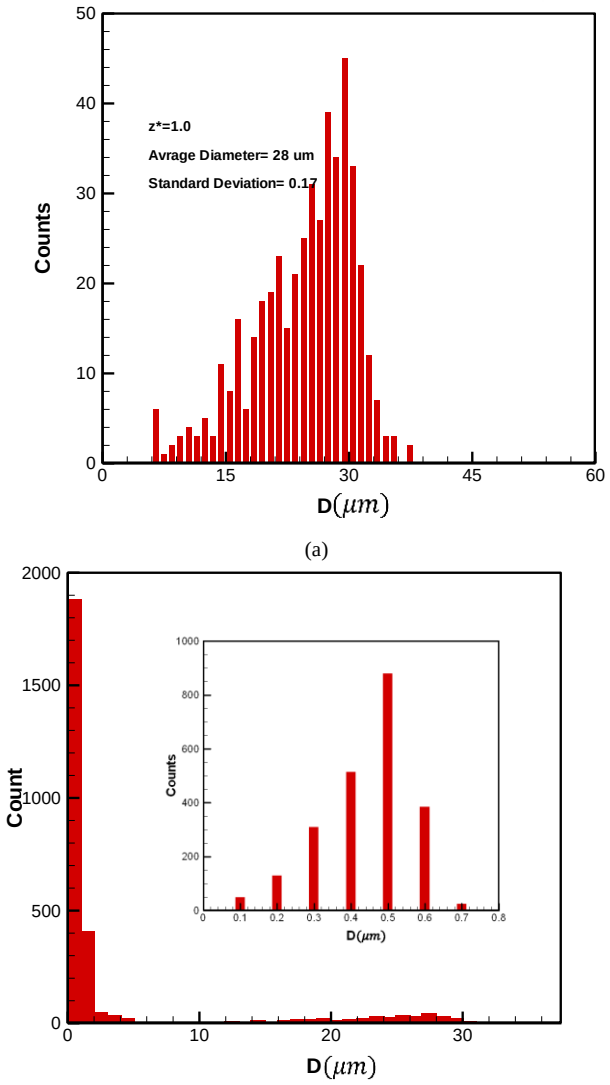

Figure 7. Comparison of the droplet size distribution in $z^* = 1$ for both (a) without and (b) with Coulomb fission.

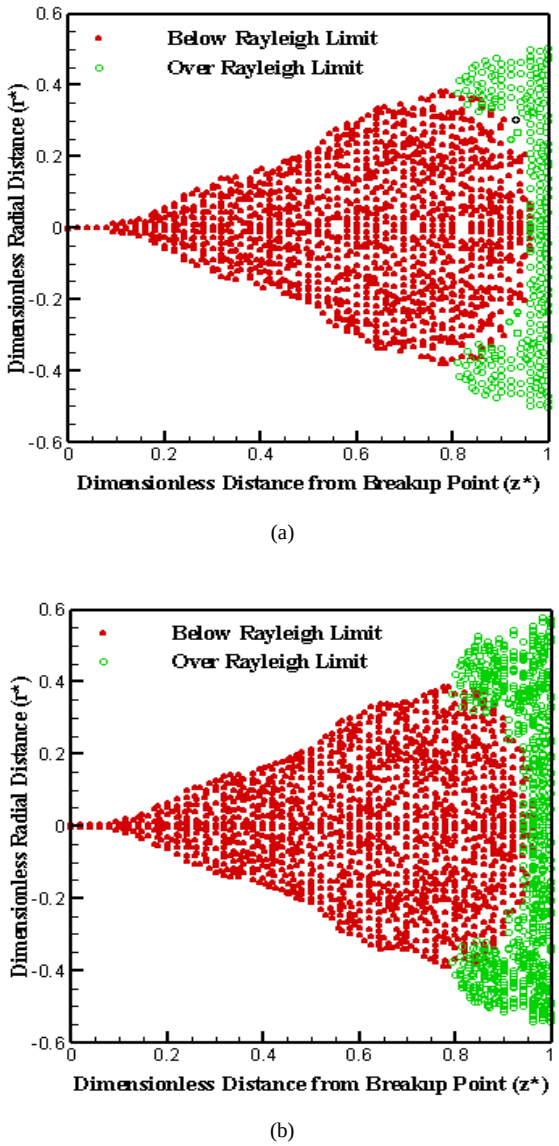

Figure 8. Comparison of the droplet position distribution in the snapshot of the electro-spray cone (a) without Coulomb fission and (b) with Coulomb fission. (The green points indicate that droplet has reached the Rayleigh limit)

Finally, the interacting force of the electric charge on the surface of the droplets reaches the Rayleigh Limit and overcomes the surface tension. At this point, the droplet surface charge density is $7.722 \times 10^{-4} \mathrm{C/m^2}$, which is the beginning of the first Coulomb fission process. At this time, the droplet is in the position $z^* = 0.77020$ and its size is $r^* = 0.488361$. The droplet trajectory and its radius variation in the path are shown in Figure 8(a). At the first stage of the fission, the primary droplet is broken up to one secondary parent droplet, with a diameter of d=1.67308 μm, and 11 small child droplets with different diameters. Child droplets removed 88.8% of the mass of the initial droplet. However, the secondary parent droplet carries 82.95% of the electric charge, and the surface charge density is reduced to $6.583 \times 10^{-4} \mathrm{C/m^2}$, which is less than the Rayleigh limit in this diameter. Small child droplets carry 17.05% of the electric charge of initial droplet and due to small size, have a high surface charge density of $5.92 \times 10^{-5} \mathrm{C/m^2}$. Spatial distribution of secondary parent droplets and child droplets after the first step Coulomb fission of droplet is shown in Figure 8(b).

5. Conclusion

This study predicted droplet Coulomb fission and trajectories of droplets in a steady spray plume, within a monodisperse EHD spray in a Lagrangian framework. The droplet fission was simulated based on the principle of minimum free energy using genetic algorithm and droplet trajectories were predicted using Lagrangian single-droplet dynamic tracking method. In the new method, unlike conventional methods, no non-physical assumptions such as the number and amount of droplets in the Colombian fission process were used. The number and position of droplets and their size were obtained only by optimizing the energy equation. Due to the distribution of droplets obtained from numerical and experimental results and the very low deviation standard of this distribution, this spray method produced highly uniform and monodisperse droplets that could be considered and used in the relevant applications. By changing the amount of applied potential, the intensity of the electric field and the volumetric flow rate, the size of these droplets could be controlled. The amount of electric charge on each droplet could also be considered in several ways: First, these droplets did not stick

together due to the charges on the surface. Second, with a suitable electric field, the proper movement of these droplets could be easily determined and controlled. Controlled Coulomb fission could also be used to obtain smaller droplets or to break larger droplets. According to the mentioned solution process, obtained results, and comparison with the data of other researchers, it was clearly seen that the numerical developed code had sufficient accuracy and precision.

References

[1] S. Boehringer, P. Ruzgys, L. Tamò, S. Šatkauskas, T. Geiser, A. Gazdhar, D. Hradetzky, A new electrospray method for targeted gene delivery, *Scientific reports*, Vol. 8, No. 1, pp. 1-12, 2018.

[2] J. B. Fenn, Electrospray wings for molecular elephants (Nobel lecture), *Angewandte Chemie International Edition*, Vol. 42, No. 33, pp. 3871-3894, 2003.

[3] X. Hou, K.-L. Choy, Synthesis and characteristics of CuInS2 films for photovoltaic application, *Thin Solid Films*, Vol. 480, pp. 13-18, 2005.

[4] R. Y. Hsu, J. H. Liao, H. W. Tien, G. R. Her, Gas chromatography electrospray ionization mass spectrometry analysis of trimethylsilyl derivatives, *Journal of Mass Spectrometry*, Vol. 51, No. 10, pp. 883-888, 2016.

[5] M. K. I. Khan, A. Nazir, A. A. Maan, Electrospraying: a novel technique for efficient coating of foods, *Food Engineering Reviews*, Vol. 9, No. 2, pp. 112-119, 2017.

[6] S. Martin, P. Garcia-Ybarra, J. Castillo, Electrospray deposition of catalyst layers with ultra-low Pt loadings for PEM fuel cells cathodes, *Journal of Power Sources*, Vol. 195, No. 9, pp. 2443-2449, 2010.

[7] K. Mohammadi, M. R. Movahhedy, S. Khodaygan, A multiphysics model for analysis of droplet formation in electrohydrodynamic 3D printing process, *Journal of Aerosol Science*, Vol. 135, pp. 72-85, 2019.

[8] A. M. Gañán-Calvo, J. M. López-Herrera, N. Rebollo-Muñoz, J. Montanero, The onset of electrospray: the universal scaling laws of the first ejection, *Scientific reports*, Vol. 6, pp. 32357, 2016.

[9] M. Cloupeau, B. Prunet-Foch, Electrohydrodynamic spraying functioning modes: a critical review, *Journal of Aerosol Science*, Vol. 25, No. 6, pp. 1021-1036, 1994.

[10] J.-P. Borra, Review on water electro-sprays and applications of charged drops with focus on the corona-assisted cone-jet mode for High Efficiency Air Filtration by wet electro-scrubbing of aerosols, *Journal of Aerosol Science*, Vol. 125, pp. 208-236, 2018.

[11] A. Ganan-Calvo, J. Lasheras, J. Dávila, A. Barrero, The electrostatic spray emitted from an electrified conical meniscus, *Journal of aerosol science*, Vol. 25, No. 6, pp. 1121-1142, 1994.

[12] O. Wilhelm, L. Mädler, S. E. Pratsinis, Electrospray evaporation and deposition, *Journal of Aerosol Science*, Vol. 34, No. 7, pp. 815-836, 2003.

[13] H. Oh, K. Kim, S. Kim, Characterization of deposition patterns produced by twin-nozzle electrospray, *Journal of Aerosol Science*, Vol. 39, No. 9, pp. 801-813, 2008.

[14] J. H. Jung, H. Oh, S. S. Kim, Numerical simulation of the deposition pattern in multiple electrohydrodynamic spraying, *Powder Technology*, Vol. 198, No. 3, pp. 439-444, 2010.

[15] W. Yang, B. Lojewski, Y. Wei, W. Deng, Interactions and deposition patterns of multiplexed electrosprays, *Journal of Aerosol Science*, Vol. 46, pp. 20-33, 2012.

[16] Z. Jiang, Y. Gan, Y. Shi, An improved model for prediction of the cone-jet formation in electrospray with the effect of space charge, *Journal of Aerosol Science*, Vol. 139, pp. 105463, 2020.

[17] J. Grifoll, J. Rosell-Llompart, Efficient Lagrangian simulation of electrospray droplets dynamics, *Journal of aerosol science*, Vol. 47, pp. 78-93, 2012.

[18] J. Grifoll, J. Rosell-Llompart, Continuous droplets' charge method for the Lagrangian simulation of electrostatic sprays, *Journal of Electrostatics*, Vol. 72, No. 5, pp. 357-364, 2014.

[19] A. M. Gañán-Calvo, N. Rebollo-Muñoz, J. Montanero, The minimum or natural rate of flow and droplet size ejected by Taylor cone–jets: physical symmetries and scaling laws, *New Journal of Physics*, Vol. 15, No. 3, pp. 033035, 2013.

[20] D. C. Taflin, T. L. Ward, E. J. Davis, Electrified droplet fission and the Rayleigh limit, *Langmuir*, Vol. 5, No. 2, pp. 376-384, 1989.

[21] W. Gu, P. E. Heil, H. Choi, K. Kim, Comprehensive model for fine Coulomb fission of liquid droplets charged to Rayleigh limit, *Applied physics letters*, Vol. 91, No. 6, pp. 064104, 2007.

[22] L. Rayleigh, XX. On the equilibrium of liquid conducting masses charged with electricity, *The London, Edinburgh, and Dublin Philosophical Magazine and Journal of Science*, Vol. 14, No. 87, pp. 184-186, 1882.

[23] A. Gomez, K. Tang, Charge and fission of droplets in electrostatic sprays, *Physics of Fluids*, Vol. 6, No. 1, pp. 404-414, 1994.

[24] J. Shrimpton, Dielectric charged drop break-up at sub-Rayleigh limit conditions, *IEEE Transactions on Dielectrics and Electrical insulation*, Vol. 12, No. 3, pp. 573-578, 2005.

[25] J. Shrimpton, Modeling dielectric charged drop break up using an energy conservation method, *IEEE Transactions on Dielectrics and Electrical Insulation*, Vol. 15, No. 5, pp. 1471-1477, 2008.

[26] D. G. Roth, A. J. Kelly, Analysis of the disruption of evaporating charged droplets, *IEEE transactions on industry applications*, No. 5, pp. 771-775, 1983.

[27] R. Clift, J. R. Grace, M. E. Weber, 2005, *Bubbles, drops, and particles*, Courier Corporation,

[28] M. Rahmanpour, R. Ebrahimi, *Numerical Simulation of Heat and Mass Transfer and Fission of Charged Droplets in an Electrohydrodynamic spray*, Thesis, K. N. Toosi University of Technology, Iran, 2017.

[29] A. H. Lefebvre, V. G. McDonell, 2017, *Atomization and sprays*, CRC press,

[30] Y. Mori, K. Hijikata, T. Nagasaki, Electrostatic atomization for small droplets of uniform diameter, *Trans. Jpn. Soc. Mech. Eng. Ser. B*, Vol. 47, pp. 1881-1890, 1981.

[31] H. Liu, M. Altan, Science and engineering of droplets: fundamentals and applications, *Appl. Mech. Rev.*, Vol. 55, No. 1, pp. B16-B17, 2002.

[32] S. R. Turns, 1996, *Introduction to combustion*, McGraw-Hill Companies,

[33] M. Rahmanpour, R. Ebrahimi, Numerical simulation of electrohydrodynamic spray with stable Taylor cone–jet, *Heat and Mass Transfer*, Vol. 52, No. 8, pp. 1595-1603, 2016.

[34] J. B. Fenn, Ion formation from charged droplets: roles of geometry, energy, and time, *Journal of the American Society for Mass Spectrometry*, Vol. 4, No. 7, pp. 524-535, 1993.

[35] R. B. Cole, 2011, *Electrospray and MALDI mass spectrometry: fundamentals, instrumentation, practicalities, and biological applications*, John Wiley & Sons,

[36] P. Kebarle, M. Peschke, On the mechanisms by which the charged droplets produced by electrospray lead to gas phase

ions, *Analytica Chimica Acta*, Vol. 406, No. 1, pp. 11-35, 2000.

[37] S. Banerjee, S. Mazumdar, Electrospray ionization mass spectrometry: a technique to access the information beyond the molecular weight of the analyte, *International journal of analytical chemistry*, Vol. 2012, 2012.

[38] Q. He, D. Fu, *The improvement of genetic algorithm and its applications for the inversion of orthorhombic anisotropic media*, in: *SEG Technical Program Expanded Abstracts 1999*, Eds., pp. 1791-1792: Society of Exploration Geophysicists, 1999.

[39] H. C. Hunter III, Studies Related to Coulombic Fissions of Charged Droplets and Hygroscopic Behavior of Mixed Particles, 2011.

[40] P. Kebarle, U. H. Verkerk, Electrospray: from ions in solution to ions in the gas phase, what we know now, *Mass spectrometry reviews*, Vol. 28, No. 6, pp. 898-917, 2009.